electronics

MDPI

Article

Temperature Dependence of Total Ionizing Dose Effects of β-Ga_2O_3 Schottky Barrier Diodes

Weili Fu [1,2], Teng Ma [1,*], Zhifeng Lei [1], Chao Peng [1], Hong Zhang [1], Zhangang Zhang [1], Tao Xiao [1,2], Hongjia Song [2], Yuangang Wang [3], Jinbin Wang [2], Zhao Fu [2] and Xiangli Zhong [2,*]

[1] Reliability Physics and Application Technology of Electronic Component Key Laboratory, China Electronic Product Reliability and Environmental Testing Research Institute, Guangzhou 511370, China
[2] National-Provincial Laboratory of Special Function Thin Film Materials, School of Materials Science and Engineering, Xiangtan University, Xiangtan 411105, China
[3] The National Key Laboratory of Solid-State Microwave Devices and Circuits, Hebei Semiconductor Research Institute, Shijiazhuang 050051, China
* Correspondence: mateng@ceprei.com (T.M.); xlzhong@xtu.edu.cn (X.Z.)

Abstract: This paper investigates the temperature-dependent effects of gamma-ray irradiation on β-Ga_2O_3 vertical Schottky barrier diodes (SBDs) under a 100 V reverse bias condition at a total dose of 1 Mrad(Si). As the irradiation dose increased, the radiation damage became more severe. The total ionizing dose (TID) degradation behavior and mechanisms were evaluated through DC, capacitance–voltage (C-V), and low-frequency noise (LFN) measurements by varying irradiation, and the test results indicated that TID effects introduced interface defects and altered the carrier concentration within the material. The impact of TID effects was more pronounced at lower temperatures compared to higher temperatures. Additionally, the annealing effect in the high-temperature experimental conditions ameliorated the growth of interface trap defects caused by irradiation. These results suggest that compared to low-temperature testing, the device exhibits higher TID tolerance after high-temperature exposure, providing valuable insights for in-depth radiation reliability studies on subsequent related devices.

Keywords: β-Ga_2O_3 Schottky barrier diode (SBD); temperature dependence; gamma-ray irradiation; interface defects; total ionizing dose (TID)

Citation: Fu, W.; Ma, T.; Lei, Z.; Peng, C.; Zhang, H.; Zhang, Z.; Xiao, T.; Song, H.; Wang, Y.; Wang, J.; et al. Temperature Dependence of Total Ionizing Dose Effects of β-Ga_2O_3 Schottky Barrier Diodes. *Electronics* **2024**, *13*, 2215. https://doi.org/10.3390/electronics13112215

Academic Editor: Francesco Driussi

Received: 18 March 2024
Revised: 28 April 2024
Accepted: 2 May 2024
Published: 6 June 2024

1. Introduction

Compared to traditional narrow-bandgap semiconductor materials like Si and GaAs, as well as other wide-bandgap semiconductor materials such as GaN and SiC, the ultra-wide-bandgap semiconductor gallium oxide exhibits exceptional characteristics, including a larger bandgap width, a stronger breakdown electric field, high-temperature resistance, and radiation resistance [1–5]. These features make it a promising material for electronic devices, particularly in high-radiation environments.

However, it is crucial to note that these electronic devices are susceptible to particle-induced deterioration or malfunction [6]. Statistics reveal that approximately 40% of satellite failures are attributed to anomalies caused by radiation effects in space. Consequently, investigating the damage mechanism of spacecraft electronic devices in the space radiation environment and establishing ground simulation test methods for space radiation effects are essential, which enable the prediction of damage caused by the space radiation environment on the ground, thereby improving the operational life and reliability of spacecraft in orbit.

For semiconductor devices made of wide-bandgap materials such as GaN and SiC, total ionizing dose (TID) radiation experiments on GaN-based diodes were conducted in 2020 by Bian et al. In their study, the diodes were subjected to cumulative doses of 1 Mrad(Si) gamma-ray irradiation at room temperature and increasing forward current

density [7]. In 2002, S. Metzger et al., reported on the linearity of the response of a SiC ultraviolet photodiode detector after a total dose of 20 kGy (air); the experiments were conducted at five constant temperatures ranging from 23 °C to 200 °C, and no significant changes were observed after testing [8]. In 2019, Pincuda et al., reported on the influence of high-temperature annealing on the threshold voltage drift in SiC MOSFETs after TID effects [9].

While recent studies have reported on the effects of protons, heavy ions, electrons, and neutron irradiation on β-Ga_2O_3 material and device properties, there is limited literature reporting on the impact of the temperature of gamma-ray irradiation on β-Ga_2O_3 SBD [10–12]. Chang et al., reported the impact of 100 MeV high-energy protons on β-Ga_2O_3-based solar-blind photodetectors, finding that a considerable number of oxygen vacancies were formed at the metal–semiconductor interface after irradiation. In 2023, R. M. Cadena et al., reported on low-energy ion-induced breakdown and single-event burnout (SEB) in β-Ga_2O_3 Schottky diodes; the study revealed fundamentally different responses among alpha particles, Cf-252, and heavy-ion irradiation. For power devices like gallium oxide diodes, Liu et al., reported the radiation effect of gamma irradiation (^{60}Co) on Au/Ni/β-Ga_2O_3 vertical Schottky barrier diodes; in addition, the carrier concentration calculated from the C–V measurements increased slightly after gamma irradiation. These results suggest that β-Ga_2O_3 SBDs have high intrinsic gamma irradiation hardness, and operating under bias voltage is inevitable. Due to the less-than-ideal thermal conductivity of gallium oxide material, studying the effects of TID under different temperature levels is crucial.

In this study, we performed temperature-controlled TID radiation experiments on β-Ga_2O_3 SBDs at low-to-high temperatures (−25 °C, 0 °C, 25 °C (room temperature), 50 °C, 75 °C, and 100 °C) using liquid nitrogen refrigeration equipment and a temperature-regulated incubator at 100 V, with a cumulative dose of 1 Mrad(Si), used to meet the test needs of temperature changes during the operation of spacecraft in orbit; the results indicate that the forward current density of the devices not only increases with the irradiation dose but also rises with the temperatures. Through analysis methods such as capacitance–voltage (C-V) testing and low-frequency noise (LFN), the impact of interface defects on device performance is quite pronounced, and high-temperature annealing provides a new approach to reducing interface trap concentration, improving the performance of gallium oxide-based devices.

2. Materials and Methods

The fabrication process of the devices unfolded as follows: Following the formation of N^- type material (net doping concentration of 3.0×10^{16} cm^{-3}, silicon-doped), the epitaxial film was grown using halide vapor-phase epitaxy (HVPE) on an N^+ type (001) crystal-phase β-Ga_2O_3 substrate (net doping concentration of 1.0×10^{19} cm^{-3}, stannum-doped), and surface defects arising during the vapor-phase epitaxial growth of the halide layer were eliminated through chemical mechanical grinding (CMP) technology. The schematic cross-sectional structure of the Schottky barrier diode (SBD) is depicted in Figure 1.

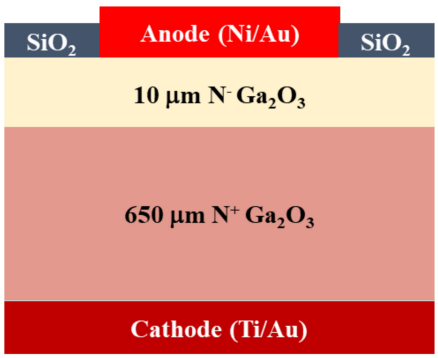

Figure 1. Schematic cross-section of β-Ga_2O_3 SBD structure.

Subsequently, the damage caused by the backside of the substrate during wafer preparation was polished. BCl_3 was applied to the substrate's backside for reactive ion etching, concluding with the evaporation of the Ti/Au stack structure to establish an ohmic contact, which was deposited by electron-beam evaporation, forming the cathode of the devices. The thicknesses were 320 μm and 200 nm. Before device fabrication, the sample was cleaned ultra-sonically several times in acetone, isopropanol, deionized water, and buffered oxide etch, and separately, a thin 200 nm SiO_2 film was grown on the epitaxial layer through plasma-enhanced chemical vapor deposition. A round metal anode was evaporated and stripped by Ni/Au evaporation in a SiO_2 window etched using a photolithography-patterned and buffered hydrofluoric acid solution. The thicknesses were 50 nm and 200 nm, and prior to the fabrication of the anode, the device was thermally oxidized in an oxygen atmosphere at a temperature of 400 °C for 20 min, which reduced the concentration of electrons in the anode edge region of the device, effectively mitigating the peak field at the edge of the device, thereby increasing the reverse breakdown voltage of the device.

For this SBD, the impact of TID effects on the electrical performance of the devices was studied at different temperatures under a reverse bias condition of 100 V, involving the following specific experimental process. The experiments were conducted at the ^{60}Co source of Xinjiang Technical Institute of Physics and Chemistry Chinese Academy of Sciences, China. Gamma-ray irradiation experiments were carried out at temperatures of −25 °C, 0 °C, 25 °C (room temperature), 50 °C, 75 °C, and 100 °C with a reverse bias condition of 100 V, and the radiation dose rate was 50 rad(Si)/s. The electrical performance, C-V, and LFN of the SBD were tested using the B1500A semiconductor parameter analyzer from Keysight Technologies and the Fs-Pro testing instrument from Primarius Electronics. Measurements were performed under all experimental conditions, at least three devices of each type and size were evaluated, and test junctions are averages. The tests were conducted offline at cumulative doses of 0 krad(Si), 300 krad(Si), 500 krad(Si), and 1 Mrad(Si).

3. Results and Discussions

In Figure 2a, it can be observed that the forward conduction current of devices increased as the cumulative radiation dose increased when experiments were conducted at 25 °C. In Figure 2b, after gamma-ray irradiation with a cumulative dose of 1 Mrad(Si), devices tested at six different temperature conditions showed varying increases in forward current density at 1 V. For instance, at 25 °C, the forward current density at 1 V increased by 25%, while at 100 °C, it increased by 72%. Therefore, the impact on the forward conduction characteristics of the devices became more pronounced with higher temperatures during the irradiation process. Given the high carrier mobility and the substantial average free path inherent in gallium oxide materials, the predominant current transport mechanism in Schottky barriers is primarily attributed to the thermal electron emission of the majority of carriers; following the theory of hot electron emission, the variation in forward current density with voltage can be expressed as described in [13–15], as follows:

$$J = A^* T^2 \exp\left(-\frac{q\phi}{kT}\right) \exp\left(-\frac{qV}{nkT}\right) = J_{sT} exp\left(-\frac{qV}{nkT}\right) \quad (1)$$

$$J_{ST} = A^* T^2 \exp\left(-\frac{q\phi}{kT}\right) A^* = \frac{4\pi q m_n{}^* k^2}{h^3} \quad (2)$$

$$\Phi = \frac{kT}{q} \ln\left(\frac{AA^* T^2}{I_s}\right) \quad (3)$$

$$n = \frac{q}{kT} \frac{\partial V}{\partial (lnJ)} \quad (4)$$

where J is the current density; T is the thermodynamic temperature; $q = 1.6 \times 10^{-19}$ C, which is the electron charge; k is the Boltzmann constant; n represents the Schottky diode

and ideal in the experiment, the ideality factor of the Schottky diode; J_{ST} is the reverse saturation current density, which is independent of the applied voltage and is a function of strong temperature dependence; Φ is the Schottky potential, the base height, where A^* is the Richardson constant and is usually taken as 40.8 A/(cm^2·K^2); m_n^* is the effective mass of the electron. We extracted the electrical parameters and the variation in the irradiated diode influenced by the data in Figure 2 and the above formulas, and the changes before and after irradiation with a cumulative dose of 1 Mrad(Si) are presented in Table 1.

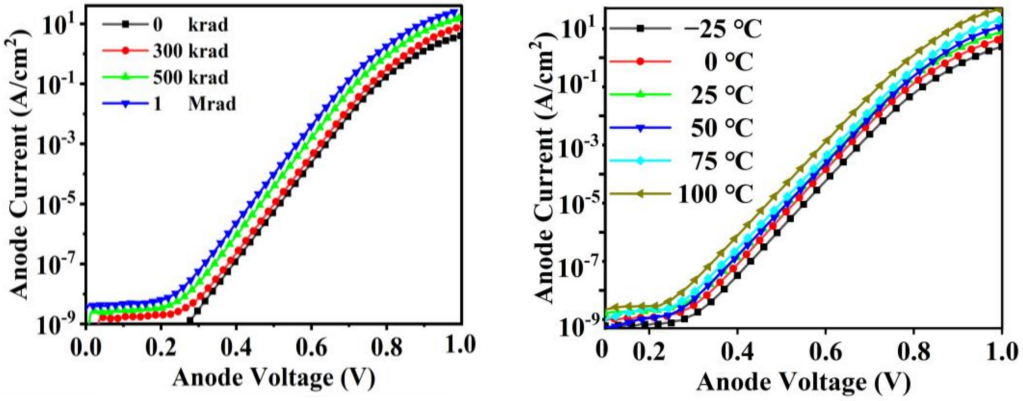

Figure 2. (**a**) Forward current density (J-V) in semi-log-scale at different doses (0 krad(Si), 300 krad(Si), 500 krad(Si), and 1 Mrad(Si)) at a temperature of room temperature and (**b**) forward current density (lgJ-V) in semi-log-scale at different temperature levels (−25 °C, 0 °C, 25 °C, 50 °C, 75 °C, and 100 °C) with a cumulative dose of 1 Mrad(Si).

Table 1. Changes in device electrical parameters before and after irradiation.

	***n* (before)**	***n* (after)**	***n***	**Φ (before)**	**Φ (after)**	**Φ**	***J***
−25 °C	1.166	1.147	−1.63%	1.06	1.01	−4.3%	+14%
0 °C	1.19	1.161	−2.44%	0.987	0.951	−3.6%	+19%
25 °C	1.172	1.153	−1.6%	1.032	0.974	−5.6%	+25%
50 °C	1.168	1.156	−1.02%	1.031	0.977	−5.2%	+44%
75 °C	1.156	1.143	−1.12%	1.102	1.057	−4.1%	+57%
100 °C	1.174	1.140	−2.90%	1.024	0.985	−3.81%	+72%

From Table 1, we can see that except for the increase in forward current density with the experimental temperature, the changes in φ and n were not significant. As the temperature increased, more electrons within the gallium oxide material gained energy, transitioning from the valence band to the conduction band to participate in conduction; simultaneously, the ionizing damage caused by irradiation increased with the accumulation of irradiation dose. These two factors contributed to the systematic changes in the forward current density of the devices. The changes in the reverse electrical characteristics of the devices are shown in Figure 3; in Figure 3a, it is shown that the reverse current density of the devices increased with the cumulative radiation dose. For this SBD, when the cathode voltage exceeded a certain critical value, the device current suddenly increased, and this reverse voltage was defined as the breakdown voltage of the diode; before the irradiation experiment, the breakdown voltage of the device was 650 V. As shown in Figure 3b, after irradiation at different temperatures, the breakdown voltage of the devices decreased; compared to that at lower temperatures, the reduction in breakdown voltage was relatively lower at higher temperatures.

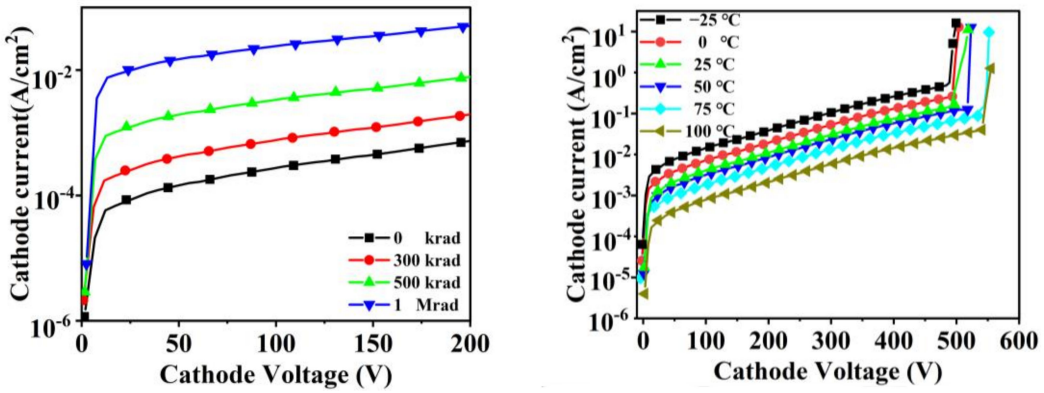

Figure 3. (**a**) Reverse current density (J-V) in semi-log-scale after different doses of gamma-ray radiation at room temperature; (**b**) reverse current density (J-V) in the semi-log-scale plot at different temperatures (−25 °C, 0 °C, 25 °C, 50 °C, 75 °C, and 100 °C) after 1 Mrad(Si) doses of gamma-ray radiation.

Reverse leakage current is a crucial parameter influencing breakdown voltage. In the SBDs, the reverse leakage current of the device increased with the accumulation of irradiation dose before reaching the reverse voltage required for breakdown. The reverse leakage current in the SBDs mainly consisted of thermal electron emission current and recombination current; the former is strongly correlated with the Schottky barrier, while the latter is influenced by carrier lifetime. From Table 1, it can be inferred that gamma-ray irradiation led to a slight reduction in the Schottky barrier height (SBH), increasing thermionic emission current, contributing to the observed slight increase in reverse leakage current and the decrease in breakdown voltage. However, in Figure 3b, it is evident that there was a slight decrease in reverse leakage current density with increasing irradiation temperature. To further understand this phenomenon, we conducted C-V tests, and the results are shown in Figure 4.

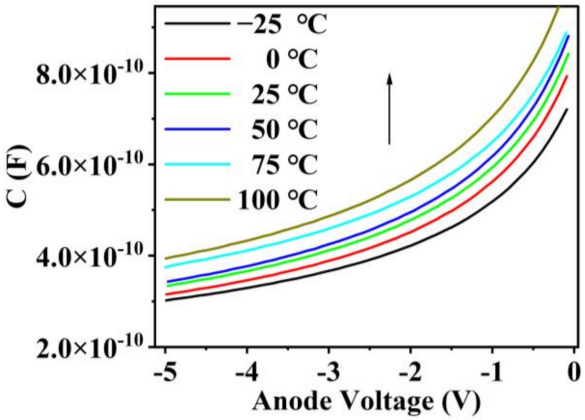

Figure 4. β-Ga_2O_3 SBD C-V plot after 1 Mrad(Si) dose of gamma-ray radiation at different temperatures (−25 °C, 0 °C, 25 °C, 50 °C, 75 °C, and 100 °C) while the frequency is 1 MHz.

The corresponding carrier concentration in the drift layer can be obtained from the following formula [16–18]:

$$N_d = -\frac{2}{q\varepsilon\varepsilon_0 A^2} \times \frac{1}{\frac{dC^{-2}}{dV}} \quad (5)$$

where N_d represents the carrier concentration; from the data in Figure 4, we extracted the specific changes in the carrier concentration of the device before and after irradiation, as shown in Table 2.

Table 2. Carrier concentration before and after irradiation in the drift layer.

	N_d (before Irradiation cm^{-3})	N_d (after Irradiation cm^{-3})	Change Magnitude
−25 °C	8.520×10^{15}	7.496×10^{15}	−12.0%
0 °C	8.416×10^{15}	7.740×10^{15}	−8.02%
25 °C	8.526×10^{15}	8.007×10^{15}	−6.08%
50 °C	8.231×10^{15}	7.875×10^{15}	−4.32%
75 °C	8.318×10^{15}	8.097×10^{15}	−2.65%
100 °C	8.532×10^{15}	8.424×10^{15}	−1.26%

As observed in Table 2, the concentration of carriers involved in conduction decreased by 12%, dropping from $8.520 \times 10^{15}/cm^3$ to $7.496 \times 10^{15}/cm^3$ after irradiation with 1 Mrad(Si) at an irradiation temperature of −25 °C. However, in devices irradiated at 100 °C, the concentration of carriers participating in conduction decreased from $8.532 \times 10^{15}/cm^3$ to $8.424 \times 10^{15}/cm^3$, showing a mere 1.26% decrease, and the carrier concentration of the device exhibited a gradient change from low temperature to high temperature. For semiconductors, the carrier concentration is mainly influenced by the material's bulk defects and interface defects. When a device is exposed to gamma-ray irradiation, it not only generates ionizing damage, leading to a transient increase in forward current, but also introduces additional hole–electron pairs inside the material, and the holes, with low mobility, migrate under applied bias to the metal–semiconductor contact, forming interface defects. Moreover, when the irradiation dose is sufficiently large, bulk defects are also introduced into gallium oxide material. The combined effects of these two types of defects impact the carrier concentration and the electrical characteristics of devices.

Electrical properties serve as external indicators of the internal structure and current conduction of electronic devices; changes in a device's internal structure can be reflected through alterations in its electrical properties. As per the above analysis, TID effects induced damage to the β-Ga_2O_3 SBDs, leading to alterations in the internal conduction characteristics of the device; these included a decrease in the ideality factor and an elevation in forward current post-turn-on. Although these electrical parameters could characterize the radiation resistance of the β-Ga_2O_3 diode, they were not very sensitive indicators due to the subtle nature of their changes.

Noise, on the other hand, is recognized for its sensitivity in reflecting various potential defects that can lead to device failure; noise analysis provides a rapid and non-destructive means of detection. As the lattice structure, electronic state, or impurity distribution of a device undergoes slow changes over time or due to stress, noise exhibits more significant increases and alterations compared to other structurally sensitive parameters (such as leakage current and ideality factor). The failure of semiconductor devices is often attributed to the presence of some underlying defects generated during the production and operation processes of the device; the noise in electronic devices is quite sensitive to the defects present in the device, and therefore, noise testing is often used to diagnose and predict the reliability of devices. Numerous research results have indicated that $1/f$ noise can serve as a sensitive parameter characterizing electronic components [19–21]. Hence, in the study of space charge regions, oxide-layer defects near the oxide semiconductor interface, and interface states, noise diagnostics prove to be a valuable technique, reflecting the degree of radiation damage more effectively than traditional electrical parameters. The test results for LFN are shown in Figure 5.

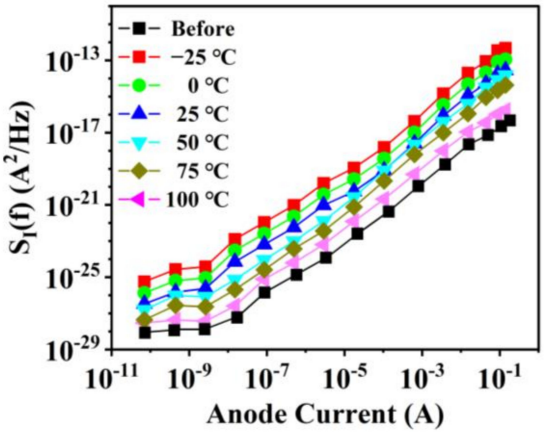

Figure 5. β-Ga_2O_3 SBD LFN plot after 1 Mrad(Si) dose of gamma-ray radiation at different temperatures (−25 °C, 0 °C, 25 °C, 50 °C, 75 °C, and 100 °C) while the frequency is 100 Hz. Before is the device without radiation.

In gallium oxide material, Ga and O atoms have high displacement threshold energies of 20.5 eV and 25.56 eV, respectively. This characteristic gives it higher radiation resistance compared to arsenide materials, and introducing bulk defects in GaAs requires a cumulative dose of gamma ray, reaching 5.45 × 10^{16} rad(Si) [22,23]. Therefore, the total dose of 1 Mrad(Si) in this experiment was not sufficient to introduce bulk defects in Ga_2O_3, a material with stronger radiation resistance; the observed changes in the noise current power spectral density in this experiment excluded the influence of bulk defects. From Figure 5, at lower temperatures, −25 °C and 0 °C, the amplitude of the LFN current power spectral density after irradiation was greater than that at room temperature. However, at higher temperatures, 50 °C, 75 °C, and 100 °C, the amplitude of the LFN current power spectral density was smaller after irradiation compared to at room temperature. Based on the three formulas for LFN in a current diode, we conducted the following analysis to study this mechanism.

Formula (1), HSU's proposed LFN carrier fluctuation model, suggests that the changes in LFN in SBDs result from the modulation of the SBH by traps or fluctuations generated by electron states in composite centers. This is primarily associated with variations in the concentration of interface defects within the material, fundamentally caused by changes in defect concentration, which in turn affect carrier concentration as follows [24]:

$$S_{I_u} = \frac{\beta^2}{f}\left(\frac{qI}{4\varepsilon_s}\right)^2\left(\frac{2h}{4\pi q}\right)^2\frac{qD_t}{6m^*N_dAW^2} \tag{6}$$

where β characterizes the carrier transport mechanism of the SBD which is equal to q/kT for thermionic emission, f is the frequency of the noise test, q is the amount of charge, I is the forward voltage at the time of the test, ε_s is the dielectric constant of the semiconductor material (gallium oxide in this test), h is Planck's constant, D_t is the defect density of the device body, m^* is the effective mass of electrons in the semiconductor material, N_d is the doping concentration after irradiation, A is the effective contact area of the device, and W is the width of the space charge region. Due to the small variation in SBH and as analyzed earlier, the influence of bulk defects is not considered in this experiment. Therefore, Equation (6) does not apply to the current study.

Regarding Formula (2), Luo et al., posit that the 1/f noise observed in SBDs is induced by fluctuations in carrier mobility within the space charge region. They propose models based on the fluctuations in mobility and diffusion coefficient, outlined as follows [25,26]:

$$S_{I_m} = \frac{\alpha I}{16\pi f}\left(\frac{1}{\beta(V_D - V_F)}\right)^{5/2}\cdot\left(\frac{q}{\mu m^*}\right)^2\left(\frac{m^*\varepsilon_s}{\pi N_d}\right)^{1/2} \tag{7}$$

where μ is the electron mobility, α is carrier mobility, V_D is the built-in potential difference of the pn junction, and V_F is the forward bias voltage. From Equation (7), it can be seen that the main variable that affected the noise power spectral density in this study was the change in carrier concentration. Combined with the data from Figures 4 and 5, our preliminary analysis indicates that the change in carrier concentration inside the devices is more pronounced at low temperatures, while the decrease in carrier concentration is smaller at high temperatures, with less fluctuation.

Regarding Formula (3), the concept of the random motion of electrons in Schottky-touched interface states was initially introduced by Jantsch. According to his argument, the interfacial current effect is directly linked to the generation–recombination of interface states. The current–noise density spectrum of the interface state can be expressed as proposed by Jantsch and others [27]. The expression for the current–noise density spectrum of the interface state, as proposed by Jantsch and others, is given by the following:

$$S_{I_r} = \frac{G\beta}{f}\left(\frac{qI}{4\varepsilon_S}\right)^2 \frac{qD_{is}}{\pi N_d WA} \tag{8}$$

where G is a constant with a value of 0.1; D_{is} is the interface state density; $q = 1.6 \times 10^{-19}$ C, which is the electron charge; k is the Boltzmann constant; β characterizes the carrier transport mechanism of the SBD which is equal to q/kT for thermionic emission; f is the frequency of the noise test; q is the amount of charge; I is the forward voltage at the time of the test; ε_S is the dielectric constant of the semiconductor material (gallium oxide in this test); h is Planck's constant; N_d is the doping concentration after irradiation; A is the effective contact area of the device; and W is the width of the space charge region. From this formula, we find that, in addition to N_d, the main variable affecting the noise power spectral density in this study is Dis, which is the interface state defect concentration. At higher temperatures, the annealing effect inside the material leads to a rearrangement of the lattice and other structures at the interface, resulting in a decrease in interface defect concentration. Simultaneously, this reduction leads to a decrease in recombination current, as observed in the changes in carrier concentration and reverse leakage current. The LFN power spectral density of the device is influenced by both carrier concentration and interface defects. Therefore, during high-temperature experiments, the noise power spectral density of the device was relatively smaller, indicating a partial recovery of the device's performance under high-temperature conditions.

Gamma-ray irradiation induces TID effects in devices, leading to transient changes in their electrical properties; it can also generate excess hole–electron pairs in gallium oxide materials and form interface defects in SBDs under the influence of voltage. Once irradiation stops, some defects rapidly return to their original state, leading to the initial steady-state decay of the damage peak, which occurs in approximately 1 s; subsequently, the damage decays to a lower level, and the presence of these defects leads to semi-permanent changes in the device's performance. At higher temperatures, defects in the Ga_2O_3 lattice undergo annealing during the irradiation process; this annealing process allows for the rearrangement and elimination of defects, reducing the defect concentration and restoring the performance parameters of the irradiated device. And without heat treatment, these defects cannot be reduced. Experimental results indicate that under the testing conditions of −25 °C and 0 °C, compared to room temperature, the concentration of interface defects in the irradiated sample is higher. Therefore, the carrier concentration and LFN exhibited larger changes. At 50 °C, 75 °C, and 100 °C, after annealing, the interface defect density was improved, leading to the partial recovery of device performance [28].

4. Conclusions

We conducted gamma-ray irradiation experiments with a cumulative dose of 1 Mrad(Si) under a reverse bias voltage of 100 V across a temperature gradient from −25 °C to 100 °C. The results indicate that the forward conduction current density of the device increases

with the cumulative irradiation dose, and the increase is more pronounced at higher temperatures. Because the reverse leakage current decreases with the increase in irradiation temperature, the reverse current of the device exhibits a different trend from the forward current. Analysis through C-V testing and LFN testing indicates that at lower temperatures, the increase in interface trap density caused by irradiation leads to an increase in interface recombination current, resulting in an elevation of leakage current and a decrease in reverse breakdown voltage. This is associated with a reduction in carrier concentration and a decrease in the noise current power spectral density, contributing to the deterioration of device performance. However, compared to room temperature, at higher temperatures, the interface states of the device undergo annealing, allowing for the reordering of interface lattices and a reduction in interface state density. This leads to a decrease in recombination current, a reduction in leakage current, and the recovery of reverse breakdown voltage. The trends in carrier concentration and noise current power spectral density changes also indicate that high-temperature annealing can improve device performance, thereby restoring its reliability.

Author Contributions: Conceptualization, C.P. and Z.Z.; Methodology, H.S. and Z.F.; Validation, H.Z.; Formal analysis, T.X.; Investigation, Z.Z.; Resources, Y.W. and J.W.; Writing—original draft, W.F.; Writing—review & editing, T.M., Z.L. and X.Z. All authors have read and agreed to the published version of the manuscript.

Funding: This research was funded by the fund of the National Natural Science Foundation of China (No. 12305299, 12275230, 12075065, and 12027813), GuangDong Basic and Applied Basic Research Foundation (No. 2022A1515111049), and Innovation Center of Radiation Application (No. KFZC2021020403).

Data Availability Statement: The datasets presented in this article are not readily available because the data are part of an ongoing study.

Acknowledgments: Acknowledgement of financial support from National Natural Science Foundation of China, GuangDong Basic and Applied Basic Research Foundation and Innovation Center of Radiation Application funds.

Conflicts of Interest: The authors declare no conflict of interest.

References

1. Tsao, J.Y.; Chowdhury, S.; Hollis, M.A.; Jena, D.; Johnson, N.M.; Jones, K.A.; Kaplar, R.J.; Rajan, S.; Van de Walle, C.G.; Bellotti, E.; et al. Ultrawide-Bandgap Semiconductors: Research Opportunities and Challenges. *Adv. Electron. Mater.* **2018**, *4*, 1600501. [CrossRef]
2. Kim, M.; Seo, J.-H.; Singisetti, U.; Ma, Z. Recent advances in free-standing single crystalline wide band-gap semiconductors and their applications: GaN, SiC, ZnO, β-Ga_2O_3, and diamond. *J. Mater. Chem. C* **2017**, *5*, 8338–8354. [CrossRef]
3. Galazka, Z. β-Ga_2O_3 for wide-bandgap electronics and optoelectronics. *Semicond. Sci. Technol.* **2018**, *33*, 113001. [CrossRef]
4. Fujita, S. Wide-bandgap semiconductor materials: For their full bloom. *Jpn. J. Appl. Phys.* **2015**, *54*, 030101. [CrossRef]
5. Mastro, M.A.; Kuramata, A.; Calkins, J.; Kim, J.; Ren, F.; Pearton, S.J. Perspective—Opportunities and Future Directions for Ga_2O_3. *ECS J. Solid State Sci. Technol.* **2017**, *6*, P356.
6. Srour, J.R.; McGarrity, J.M. Radiation effects on microelectronics in space. *Proc. IEEE* **1988**, *76*, 1443–1469. [CrossRef]
7. Bian, Z.; Su, K.; Zhang, J.; Zhao, S.; Zhou, H.; Zhang, W.; Zhang, Y.; Zhang, T.; Chen, J.; Dang, K.; et al. Gamma irradiation impact on GaN quasi-vertical Schottky barrier diodes. *J. Phys. D Appl. Phys.* **2020**, *53*, 045103. [CrossRef]
8. Metzger, S.; Henschel, H.; Kohn, O.; Lennartz, W. Silicon carbide radiation detector for harsh environments. *IEEE Trans. Nucl. Sci.* **2002**, *49*, 1351–1355. [CrossRef]
9. Pintacuda, F.; Massetti, S.; Muschitiello, M.; Cantarella, V. TID test results of radiation hardened SiC MOS structures pre-temperature stressed. In Proceedings of the 2019 European Space Power Conference (ESPC), Juan-Les-Pins, France, 30 September–4 October 2019; pp. 1–4.
10. Chang, M.M.; Guo, D.Y.; Zhong, X.L.; Zhang, F.B.; Wang, J.B. Impact of 100 MeV high-energy proton irradiation on β-Ga_2O_3 solar-blind photodetector: Oxygen vacancies formation and resistance switching effect. *J. Appl. Phys.* **2022**, *132*, 123105. [CrossRef]
11. Konishi, K.; Goto, K.; Murakami, H.; Kumagai, Y.; Kuramata, A.; Yamakoshi, S.; Higashiwaki, M. 1-kV vertical Ga_2O_3 field-plated Schottky barrier diodes. *Appl. Phys. Lett.* **2017**, *110*, 103506. [CrossRef]
12. Polyakov, A.Y.; Smirnov, N.B.; Shchemerov, I.V.; Pearton, S.J.; Ren, F.; Chernykh, A.V.; Lagov, P.B.; Kulevoy, T.V. Hole traps and persistent photo capacitance in proton irradiated β-Ga_2O_3 films doped with Si. *APL Mater.* **2018**, *6*, 096102. [CrossRef]

13. Liu, M.; Hua, M.; Tian, X.; Wang, Z.; Gao, H.; Wang, W.; Chen, Y.; Zhang, C.; Zhao, S.; Feng, Q.; et al. Effect of gamma irradiation on β-Ga_2O_3 vertical Schottky barrier diode. *Appl. Phys. Lett.* **2023**, *123*, 212103. [CrossRef]
14. Holmes-Siedle, A.G.; Adams, L. *Handbook of Radiation Effects*; Oxford University Press: Oxford, UK, 1993.
15. Sheoran, H.; Kumar, V.; Singh, R. A Comprehensive Review on Recent Developments in Ohmic and Schottky Contacts on Ga_2O_3 for Device Applications. *ACS Appl. Electron. Mater.* **2022**, *4*, 2589–2628. [CrossRef]
16. Sze, S.M.; Li, Y.; Ng, K.K. *Physics of Semiconductor Devices*; Nework Wiley: Hoboken, NJ, USA, 1981.
17. Zheng, X.-F.; Dong, S.-S.; Ji, P.; Wang, C.; He, Y.-L.; Lv, L.; Ma, X.-H.; Hao, Y. Characterization of bulk traps and interface states in AlGaN/GaN heterostructure under proton irradiation. *Appl. Phys. Lett.* **2018**, *112*, 233504. [CrossRef]
18. Ai, W.-S.; Liu, J.; Feng, Q.; Zhai, P.-F.; Hu, P.-P.; Zeng, J.; Zhang, S.-X.; Li, Z.-Z.; Liu, L.; Yan, X.-Y.; et al. Degradation of β-Ga_2O_3 Schottky barrier diode under swift heavy ion irradiation. *Chin. Phys. B* **2021**, *30*, 056110. [CrossRef]
19. Vandamme, L.K.J. Noise as a diagnostic tool for quality and reliability of electronic devices. *IEEE Trans. Electron Devices* **1994**, *41*, 2176–2187. [CrossRef]
20. Zhuang, Y.; Du, L. 1/f noise as a reliability indicator for subsurface Zener diodes. *Microelectron. Reliab.* **2002**, *42*, 355–360. [CrossRef]
21. Yiqi, Z.; Qing, S. 1f noise as a prediction of long-term instability in integrated operational amplifiers. *Microelectron. Reliab.* **1996**, *36*, 189–193. [CrossRef]
22. Khanna, S.M.; Webb, J.; Tang, H.; Houdayer, A.J.; Carlone, C. 2 MeV proton radiation damage studies of gallium nitride films through low temperature photoluminescence spectroscopy measurements. *IEEE Trans. Nucl. Sci.* **2000**, *47*, 2322–2328. [CrossRef]
23. Khanna, R.; Han, S.Y.; Pearton, S.J.; Schoenfeld, D.W.; Schoenfeld, W.V.; Ren, F.J.A.P.L. High dose Co-60 gamma irradiation of InGaN quantum well light-emitting diodes. *Appl. Phys. Lett.* **2005**, *87*, 212107. [CrossRef]
24. Hsu, T.S. Low-frequency excess noise in metal—Silicon Schottky barrier diodes. *IEEE Trans. Electron Devices* **1970**, *17*, 496–506. [CrossRef]
25. Luo, M.Y.; Bosman, G.; Ziel, A.V.D.; Hench, L.L. Theory and experiments of 1/f noise in Schottky-barrier diodes operating in the thermionic-emission mode. *IEEE Trans. Electron Devices* **1988**, *35*, 1351–1356. [CrossRef]
26. Schiebel, R.A. A model for 1/f noise in diffusion current based on surface recombination velocity fluctuations and insulator trapping. *IEEE Trans. Electron Devices* **1994**, *41*, 768–778. [CrossRef]
27. Jantsch, O. Flicker (1/f) noise generated by a random walk of electrons in interfaces. *IEEE Trans. Electron Devices* **1987**, *34*, 1100–1115. [CrossRef]
28. Zuleeg, R. Radiation effects in GaAs FET devices. *Proc. IEEE* **1989**, *77*, 389–407. [CrossRef]